Mean field and Monte Carlo studies of the magnetization-reversal transition in the Ising model

February 6, 2008

Arkajyoti Misra[1] and Bikas K Chakrabarti[2]
Saha Institute of Nuclear Physics, 1/AF Bidhannagar, Calcutta 700 064, India.

Abstract

Detailed mean field and Monte Carlo studies of the dynamic magnetization-reversal transition in the Ising model in its ordered phase under a competing external magnetic field of finite duration have been presented here. Approximate analytical treatment of the mean field equations of motion shows the existence of diverging length and time scales across this dynamic transition phase boundary. These are also supported by numerical solutions of the complete mean field equations of motion and the Monte Carlo study of the system evolving under Glauber dynamics in both two and three dimensions. Classical nucleation theory predicts different mechanisms of domain growth in two regimes marked by the strength of the external field, and the nature of the Monte Carlo phase boundary can be comprehended satisfactorily using the theory. The order of the transition changes from a continuous to a discontinuous one as one crosses over from coalescence regime (stronger field) to nucleation regime (weaker field). Finite size scaling theory can be applied in the coalescence regime, where the best fit estimates of the critical exponents are obtained for two and three dimensions.

[1] email : arko@cmp.saha.ernet.in
[2] email : bikas@cmp.saha.ernet.in

1 Introduction

The study of the response of pure Ising systems under the action of a time-dependent external magnetic field has been of recent interest in statistical physics [1][2][3]. A whole class of dynamic phase transitions emerged from the study of such driven spin systems under different time dependences of the driving field. A mean field study was initially proposed by Tome and Oliveira [4] where the time dependence of the external perturbation was periodic. Subsequently, through extensive Monte Carlo studies, the existence of a dynamic phase transition under periodic magnetic field was established and properly characterized [5][6][7]. Later, efforts were made to investigate the response of such systems under magnetic fields which are of the form of a 'pulse' or in other words applied for a finite duration of time. All the studies with pulsed fields were made on a system below its static critical temperature T_c^0, where the equilibrium state has got a prevalent order along a particular direction. The pulse is called 'positive' when it is applied along the direction of the prevalent order and 'negative' when applied in opposition. The results for the positive pulse case was analyzed by extending appropriately the finite size scaling technique to this finite time window case, and it did not involve any new phase transition or introduced any new thermodynamic scale [8]. However a negative field competes with the existing order and depending on the strength h_p and duration Δt of the pulse, the system may show a transition from one ordered state with equilibrium magnetization $+m_0$ (say) to the other equivalent ordered state with equilibrium magnetization $-m_0$ [9]. This transition is called here the "magnetization-reversal" transition. It may be noted that a magnetization-reversal phenomenon trivially occurs in the limit $\Delta t \to \infty$ for any non vanishing value of h_p at any $T < T_c^0$. However, this is a limiting case of the transition, which is studied here only for finite Δt. In our studies the magnetization-reversal need not occur during the presence of the external field. In fact, it will be shown later that the closer one approaches to the threshold value h_p^c of the pulse strength longer is the time taken by the system, after the field is withdrawn, to relax to the final ordered state. We report here in details the various results obtained for this dynamic magnetization-reversal transition in pure Ising model in two and three dimensions.

The model we studied here is the Ising model with nearest neighbour interaction under a time dependent external magnetic field, described by the Hamiltonian

$$H = -\frac{1}{2}\sum_{[ij]} J_{ij} S_i S_j - \sum_i h_i(t) S_i, \tag{1}$$

where J_{ij} is the cooperative interaction between the spins at sites i and j respectively and each nearest-neighbour pair denoted by $[\ldots]$ is counted twice in the summation. We consider the system at temperatures only below its static critical temperature ($T < T_c^0$). The external field is applied after the system is brought

to equilibrium characterized by an equilibrium magnetization $m_0(T)$. The field is uniform in space ($h_i(t) = h(t)$ for all i) and its time dependence is given by

$$\begin{aligned} h(t) &= -h_p \quad , \quad \text{for } t_0 \leq t \leq t_0 + \Delta t \\ &= 0 \quad , \quad \text{otherwise.} \end{aligned} \tag{2}$$

Typical responses of the time dependent magnetization $m(t)$ under different $h(t)$ are shown in figure 1. As mentioned before, for appropriate combination of h_p and Δt, magnetization-reversal transition occurs when the system makes a transition from one ordered state to another. This transition can be observed at any dimension d greater than unity for systems with short range interactions. This is because one has to work at temperatures $T < T_c^0$ where, in absence of a symmetry breaking field, the free energy landscape has got two equivalent minima at magnetizations $m = \pm m_0$. A phase boundary in the $h_p - \Delta t$ plane gives the minimal combination of the two parameters at a particular temperature $T(< T_c^0)$ required to bring about the transition.

A full numerical solution as well as an analytical treatment in the linear limit of the dynamic mean field equation of motion shows the existence of length and time scale divergences at the transition phase boundary [10]. The divergence of length and time scales is also observed in Monte Carlo (MC) simulation study of Ising model with nearest neighbour interaction evolving under a negative pulse through single spin flip Glauber dynamics [3]. The phase diagram for the transition was obtained for both MF and MC studies. While the phase boundaries for the two cases are qualitatively of similar nature, there exists a major difference which can be accounted for by considering the presence of fluctuations in the simulations. In the MC study, there exists two distinct time scales in the problem : (i) the nucleation time τ_N is the time taken by the system to leave the metastable state under the influence of the external magnetic field and (ii) the relaxation time τ_R is the time taken by the system to reach the final equilibrium state after the external field is withdrawn. While τ_N is controlled by the strength h_p of the external pulse and is bounded by its duration Δt which is finite, τ_R is the time scale that diverges at the magnetization-reversal phase boundary. According to the classical nucleation theory (CNT) [11], there can be two distinct mechanisms for the growth of domains or droplets depending on the strength of the external field. Under the influence of weaker external magnetic fields, only a single droplet grows to span the entire system and this is called the single-droplet (SD) or the nucleation regime. On the other hand, under stronger magnetic fields, many small droplets can grow simultaneously and eventually coalesce to form a system spanning droplet. This is called the multi-droplet (MD) or the coalescence regime. The crossover from SD to MD regime takes place at the dynamic spinodal field or $h_{DSP}(L, T)$ which is a function of system size L and temperature T. The nucleation time τ_N changes abruptly as one crosses over from SD to MD regime even along the same phase boundary. The nature of the transition too changes from a continuous one in the MD regime to a discontinuous

nature in the SD regime. All our simulation observations for the dynamic phase boundary compare well with those suggested by the CNT. The investigations about the relaxation time τ_R and the correlation length ξ are also discussed here. The application of scaling theory in the MD regime gives the estimates of the critical exponents for this dynamic transition. The organization of the paper in as follows : We discuss the MF results in the next section and the MC results for square and simple cubic lattices in section 3. A brief summary and concluding remarks are given in section 4.

2 Mean field study

The master equation for a system of N Ising spins in contact with a heat bath evolving under Glauber single spin flip dynamics can be written as [12]

$$\begin{aligned} \frac{d}{dt}P\left(S_1,\cdots,S_N;\,t\right) &= -\sum_j W_j(S_j)P\left(S_1,\ldots,S_N;\,t\right) \\ &+ \sum_j W_j(-S_j)P\left(S_1,\ldots,-S_j,\ldots,S_N;\,t\right), \end{aligned} \tag{3}$$

where $P\left(S_1,\cdots,S_N;\,t\right)$ is the probability to find the spins in the configuration $(S_1,\cdots,S_N)$ at time t and $W_j(S_j)$ is the probability of flipping of the jth spin. Satisfying the condition of detailed balance one can write the transition probability as

$$W_j(S_j) = \frac{1}{2\lambda}\left[1 - S_j \tanh\left(\frac{\sum_i J_{ij}S_i(t) + h_j}{T}\right)\right], \tag{4}$$

where λ is a temperature dependent constant. Defining the spin expectation value as

$$m_i = \langle S_i \rangle = \sum_{\{S\}} S_i P\left(S_1,\ldots,S_N;\,t\right), \tag{5}$$

where the summation is carried over all possible spin configurations, one can write

$$\lambda\frac{dm_i}{dt} = -m_i + \left\langle \tanh\left(\frac{\sum_j J_{ij}S_j + h_i}{T}\right)\right\rangle. \tag{6}$$

Under the mean field approximation (6) can be written after a Fourier transform as

$$\lambda\frac{dm_q(t)}{dt} = -m_q(t) + \tanh\left(\frac{J(q)m_q(t) + h_q(t)}{T}\right), \tag{7}$$

where $J(q)$ is the Fourier transform of J_{ij}. Equation (7) is not analytically tractable and one can only look for solutions in the small m_q limit where terms linear in m_q are dominant. The linearized equation of motion, therefore, can be written as

$$\frac{dm_q(t)}{dt} = \lambda^{-1}\left[\left(K(q)-1\right)m_q(t) + \frac{h_q(t)}{T}\right], \tag{8}$$

where $K(q) = J(q)/T$. When we are concerned only with the homogeneous magnetization, we consider the $q = 0$ mode of the equation and writing $m_{q=0} = m$ and $h_{q=0} = h$, we get

$$\frac{dm}{dt} = \lambda^{-1}\left[\left(K(0)-1\right)m(t) + \frac{h(t)}{T}\right]. \tag{9}$$

In the mean field approximation $K(0) = T_c^{MF}/T$ with $T_c^{MF} = J(0)$ and for small q, $K(q) \simeq K(0)\,(1-q^2)$. Differentiating (7) with respect to the external field, we get the rate equation for the dynamic susceptibility $\chi_q(t)$ as

$$\lambda\frac{d\chi_q(t)}{dt} = -\chi_q(t) + \left(\frac{J(q)\chi_q(t)+1}{T}\right)\ \mathrm{sech}^2\left[\frac{J(q)m_q(t)+h_q(t)}{T}\right], \tag{10}$$

which in the linear limit can be written as

$$\frac{d\chi_q(t)}{dt} = \lambda^{-1}\left[\left(K(q)-1\right)\chi_q(t) + \frac{1}{T}\right]. \tag{11}$$

Before we proceed with the solutions of these dynamical equations, we divide the entire time zone in three different regimes : (I) $0 < t < t_0$, where $h(t) = 0$ (II) $t_0 \le t \le t_0 + \Delta t$, where $h(t) = -h_p$ and (III) $t_0 + \Delta t < t < \infty$, where $h(t) = 0$ again. We note that (9) can be readily solved separately for the three regions as the boundary conditions are exactly known. In region I, $dm/dt = 0$ and the solution of the linearized (9) becomes trivial. We, therefore, use the solution of (7) in region I ($m_0 = \tanh\left(m_0 T_c^{MF}/T\right)$) as the initial value of m for region II. Integrating (9) in region II, we then get

$$m(t) = \frac{h_p}{\Delta T} + \left(m_0 - \frac{h_p}{\Delta T}\right)\exp\left[b\Delta T\,(t-t_0)\right], \tag{12}$$

where $b = 1/\lambda T$ and $\Delta T = T_c^{MF} - T$. It is to be noted that in order to justify the validity of the linearization of (7) one must keep the factor inside the exponential of (12) small. This restricts the linear theory to be valid at temperatures close to T_c^{MF} and for small values of Δt. Writing $m_w \equiv m(t_0 + \Delta t)$, we get from (12)

$$m_w = \frac{h_p}{\Delta T} + \left(m_0 - \frac{h_p}{\Delta T}\right)e^{b\Delta T\Delta t}. \tag{13}$$

It is to be noted here that in absence of fluctuations, the sign of $m_w(h_p, \Delta t)$ solely decides which of the two final equilibrium states will be chosen by the system after the withdrawal of the pulse. At $t = t_0 + \Delta t$, if $m_w > 0$, the system goes back to $+m_0$ state and if $m_w < 0$, magnetization-reversal transition occurs and the system eventually chooses the $-m_0$ state (see figure 1). Thus setting $m_w = 0$, we obtain the threshold value of the pulse strength at the mean field phase boundary for this dynamic phase transition. At any T, combinations of h_p and Δt below the phase boundary cannot induce the magnetization-reversal transition, while those above it can induce the transition. From (13) therefore we can write the equation of the mean field phase boundary for the magnetization-reversal transition as

$$h_p^c(\Delta t, T) = \frac{\Delta T m_0}{1 - e^{-b\Delta T \Delta t}}. \tag{14}$$

Figure 2 shows phase boundaries at different T obtained from (14) and compares those to the phase boundaries obtained from the numerical solution of the full dynamical equation (7). The phase boundaries obtained under linear approximation match quite well with those obtained numerically for small values of Δt and at temperatures close to T_c^{MF}, which is the domain of validity of the linearized theory as discussed before. In region III, we again have $h(t) = 0$ and solution of (9) leads to

$$m(t) = m_w \exp\left[b\Delta T \left\{t - (t_0 + \Delta t)\right\}\right]. \tag{15}$$

We define the relaxation time τ_R^{MF}, measured from $t = t_0 + \Delta t$, as the time required to reach the final equilibrium state characterized by magnetization $\pm m_0$ in region III (see figure 1). From (15) therefore we can write

$$\begin{aligned} \tau_R^{MF} &= \frac{1}{b\Delta T} \ln\left(\frac{m_0}{|m_w|}\right) \\ &\sim -\left(\frac{T}{T_c^{MF} - T}\right) \ln|m_w|. \end{aligned} \tag{16}$$

A point to note is that $m(t)$ in (15) grows exponentially with t and therefore in order to confine ourselves to the linear regime of $m(t)$, m_0 must be small (T close to T_c^{MF}) and $t \leq \tau_R^{MF}$. The factor $\left(T_c^{MF} - T\right)^{-1}$ gives the usual critical slowing down for the static transition at $T = T_c^{MF}$. However, even for $T \ll T_c^{MF}$, τ_R^{MF} diverges at the magnetization-reversal phase boundary where m_w vanishes. Figure 3 shows the divergence of τ_R^{MF} against m_w as obtained from the numerical solution of the full mean field equation of motion (7) and compares it with that obtained from (16).

Solution of $\chi_q(t)$ is more difficult as all the boundary conditions are not directly known. However, $\chi_q(t)$ can be expressed in terms of $m(t)$ and the solution

of the resulting equation will then have the t dependence coming through $m(t)$, which we have solved already. Dividing (10) by (7) we get

$$\frac{d\chi_q(t)}{dm(t)} = \frac{-\chi_q(t) + \left(\frac{J(q)\chi_q(t)+1}{T}\right) \operatorname{sech}^2\left[\frac{J(q)m_q(t)+h_q(t)}{T}\right]}{-m_q(t) + \tanh\left(\frac{J(q)m_q(t)+h_q(t)}{T}\right)}, \tag{17}$$

which can be rewritten in the linear limit as

$$\frac{d\chi_q}{\chi_q + \Gamma} = a_q \frac{dm}{m + h(t)/\Delta t}, \tag{18}$$

where $\Gamma = 1/T\,(K(q) - 1)$ and $a_q = (K(q) - 1)\,/\,(K(0) - 1) \simeq 1 - q^2/\Delta T$ for small q.

In region II, solution of (18) can be written as

$$\chi_q(t) = -\Gamma + \left(\chi_q^s + \Gamma\right)\left[\frac{m(t) - h_p/\Delta T}{m_0 - h_p/\Delta T}\right]^{a_q}, \tag{19}$$

where χ_q^s is the equilibrium value of susceptibility in region I. Solving (18) in region III with the initial boundary condition $m\,(t_0 + \Delta t) = m_w$, we get

$$\begin{aligned} \chi_q(t) &= -\Gamma + (\chi_q\,(t_0 + \Delta t) + \Gamma)\left(\frac{m(t)}{m_w}\right)^{a_q} \\ &= -\Gamma + \left(\chi_q^s + \Gamma\right)\left(\frac{m(t)}{m_w}\right)^{a_q} e^{b\Delta T \Delta t a_q}, \end{aligned} \tag{20}$$

where use has been made of (19) and (13). The dominating q dependence in $\chi_q(t)$ is coming from $(1/m_w)^{a_q}$ when $m_w \to 0$ as one approaches the phase boundary. The singular part of the dynamic susceptibility can then be written as

$$\chi_q(t) = \left(\chi_q^s + \Gamma\right) \exp\left[-q^2\left(\xi^{MF}\right)^2\right], \tag{21}$$

where for small values of m_w the correlation length ξ^{MF} is given by [10]

$$\xi^{MF} \equiv \xi^{MF}\,(m_w) = \left[\frac{T_c}{\Delta T} \ln\left(\frac{1}{|m_w|}\right)\right]^{\frac{1}{2}}. \tag{22}$$

Thus the length scale also diverges at the magnetization-reversal phase boundary and this can be demonstrated even using the linearized mean field equation of motion. Equations (16) and (22) can now be used to establish the following relation between the diverging time and length scales :

$$\tau_R^{MF} \sim \frac{T}{T_c}\left(\xi^{MF}\right)^2, \tag{23}$$

which leads to a dynamical critical exponent $z = 2$. It may be noted that these divergences in τ_R^{MF} and ξ^{MF} are shown to occur for any $T < T_C^{MF}$, and these dynamic relaxation time and correlation length defined for the magnetization-reversal transition exist only for $T < T_c^{MF}$.

It may further be noted from (21) that $\chi_q(t) \to 0$ as $\xi^{MF} \to \infty$, thereby producing a minimum of χ_q at the phase boundary. The absence of any divergence in the susceptibility is due to the fact that at $t = t_0 + \Delta t$, there remains no contribution of m_w in $\chi_q(t)$ as is evident from (20). However, numerical solution of (17) for $q = 0$ mode shows a clear singularity in the homogeneous susceptibility χ_0 at the magnetization-reversal phase boundary ($m_w = 0$), as depicted in figure 4. One can also have a numerical estimate of ξ^{MF} by solving (17) for different values of q. Figure 5 shows plots of $\chi_q(t)$ against m_w for different values of q. The inset of figure 5 shows the variation of $\left(\xi^{MF}\right)^{-2}$ against $(\ln|m_w|)^{-1}$, where ξ^{MF} was obtained by fitting the data of figure 5 with straight lines. It is clearly seen from the inset that for small values of m_w the linear approximation agrees quite well with the numerical results.

3 Monte Carlo Study

We now study the transition using Monte Carlo simulation with single spin-flip Glauber dynamics [13]. Working at a temperature below the static critical temperature ($T_c^0 \simeq 2.27$ and 4.51 [14] in units of the nearest neighbour interaction strength J for square and simple cubic lattices respectively), the system is prepared by evolving the initial state (say with all spins up) under Glauber dynamics for the temperature T. The evolution time t_0 is usually taken to be sufficiently larger than the static relaxation time at T to ensure that the system reaches an equilibrium state with magnetization m_0 before the external magnetic field is applied at time $t = t_0$. The magnetization $m(t)$ starts decreasing from its initial value m_0 due to the effect of the competing field during the period $t_0 \le t \le t_0 + \Delta t$, and it assumes the value m_w at $t = t_0 + \Delta t$. Due to presence of fluctuations, $m_w < 0$ does not necessarily lead to a magnetization-reversal whereas even for $m_w > 0$ fluctuations can give rise to a magnetization-reversal. This is in contrast with the mean field case, where due to the absence of any fluctuation the sign of m_w solely determines the final state. In the MC study, however, on an average the final state is determined by the sign of m_w (see figure 1). The magnetization-reversal transition phase boundary therefore again corresponds to $m_w = 0$.

Figure 6 shows phase boundaries at different temperatures for square and simple cubic lattices. The data points for $d = 2$ are averaged over 500 different Monte Carlo runs (MCR) and those for $d = 3$ are averaged over 150 MCR. A qualitative difference between the MF and the MC phase boundaries may be noted here. In the former, even for $\Delta t \to \infty$, due to the absence of fluctuations,

h_p must be greater than the non-zero coercive field to bring about the transition and therefore the phase boundaries flatten for larger values of Δt. However, in real systems fluctuations are present and even an infinitesimal strength of the pulse, if applied for very long time, can bring about the transition. This is evident from the asymptotic nature of the phase boundaries for large values of Δt.

It is instructive to look at the classical theory of nucleation to understand the nature of the MC phase diagram of the magnetization-reversal transition. A typical configuration of a ferromagnet, below its static critical temperature T_c^0, consists of droplets or domains of spins oriented in the same direction, in a sea of oppositely oriented spins. According to CNT, the equilibrium number of droplets consisting of s spins is given by $n_s = N \exp(-\epsilon_s/T)$, where ϵ_s is the free energy of formation of a droplet containing s spins and N is a normalization constant. In presence of a negative external magnetic field h, the free energy can be written as $\epsilon_s = -2hs + \sigma s^{(d-1)/d}$, where the shape of the droplet is assumed to be spherical and $\sigma(T)$ is the temperature dependent surface tension. Droplets of size greater than a critical value s_c are favoured to grow, where $s_c = [\sigma(d-1)/(2d\,|h|)]^d$ is obtained by maximizing ϵ_s. The number of supercritical droplets is therefore given by $n_{s_c} = N \exp\left[-\Lambda_d \sigma^d\,|h|^{1-d}/T\right]$, where Λ_d is a constant depending on dimension only. In the SD regime, where a single supercritical droplet grows to engulf the whole system, the nucleation time is inversely proportional to the nucleation rate I. According to the Becker-Döring theory, I is proportional to n_{s_c} and therefore one can write

$$\tau_N^{SD} \propto I^{-1} \propto \exp\left[\frac{\Lambda_d \sigma^d}{T\,|h|^{d-1}}\right].$$

However, in the MD regime the nucleation mechanism is different and in this regime many supercritical droplets grow simultaneously and eventually coalesce to create a system spanning droplet. The radius $s_c^{1/d}$ of a supercritical droplet grows linearly with time t and thus $s_c \propto t^d$. For a steady rate of nucleation, the rate of change of magnetization is It^d. For a finite change Δm of the magnetization during the nucleation time τ_N^{MD}, one can write

$$\Delta m \propto \int_0^{\tau_N^{MD}} It^d dt = I\left(\tau_N^{MD}\right)^{d+1}.$$

Therefore, in the MD regime one can write [15][16]

$$\tau_N^{MD} \propto I^{-1/(d+1)} \propto \exp\left[\frac{\Lambda_d \sigma^d}{T(d+1)\,|h|^{d-1}}\right].$$

During the time $t_0 \leq t \leq t_0 + \Delta t$, when the external field remains 'on', the only relevant time scale in the system is the nucleation time. The magnetization reversal phase boundary gives the threshold value h_p^c of the pulse strength which,

within time Δt, brings the system from an equilibrium state with magnetization $+m_0$ to a non-equilibrium state with magnetization $m_w = 0_-$, so that eventually the system evolves to the equilibrium state with magnetization $-m_0$. The field driven nucleation mechanism takes place for $t_0 \leq t \leq t_0 + \Delta t$ and therefore equating the above nucleation times with Δt, one gets the for the magnetization-reversal phase boundary

$$\begin{aligned} \ln(\Delta t) &= c_1 + C\left[h_p^c\right]^{1-d}, && \text{in the SD regime} \\ &= c_2 + C\left[h_p^c\right]^{1-d}/(d+1), && \text{in the MD regime} \end{aligned} \tag{24}$$

where $C = \Lambda_d \sigma^d / T$ and c_1, c_2 are constants. Therefore a plot of $\ln(\Delta t)$ against $\left[h_p^c\right]^{d-1}$ would show two different slopes corresponding to the two regimes [17]. Figure 7 shows these plots and it indeed have two distinct slopes for both $d = 2$ (figure 7(a)) and $d = 3$ (figure 7(c)) at sufficiently high temperatures, where both the regimes are present. The ratio R of the slopes corresponding to the two regimes has got values close to 3 for $d = 2$ and close to 4 for $d = 3$, as suggested by (24). The value of h_{DSP} is obtained from the point of intersection of the straight lines fitted to the two regimes. At lower temperatures, however, the MD region is absent and the phase diagram here is marked by a single slope as shown in figures 7(b) and 7(d).

Once the pulse is withdrawn, the system relaxes to one of the two equilibrium states. The closer one leaves the system to the phase boundary ($m_w \to 0$), larger is the relaxation time τ_R. However, unlike the mean field case, the MC relaxation time falls off exponentially with $|m_w|$ away from the phase boundary. Figure 8 shows the growth of τ_R as $m_w \to 0$ at a particular T and for a particular Δt. Typical number of MCR used to obtain the data is 400 for $L = 40$ and 25 for $L = 400$. The best fitted curve through the data points shows the relaxation behaviour as follows :

$$\tau_R \sim \kappa(T, L) e^{-\mu(T)|m_w|}, \tag{25}$$

where $\kappa(T, L)$ is a constant depending on temperature and system size and $\mu(T)$ is a constant depending on temperature only. It may be noted from (25) that $\tau \to \kappa(T, L)$ as $m_w \to 0$. Therefore the true divergence at the phase boundary (where $m_w = 0$) of the relaxation time depends on the nature of $\kappa(T, L)$. The inset of figure 8 shows the sharp growth of $\kappa(T, L)$ with the system size. The relaxation time τ_R therefore diverges in the thermodynamic limit ($L \to \infty$) through the constant κ. It may be noted that this divergence of τ_R at the dynamic magnetization-reversal phase boundary occurs even at temperatures far below the static critical temperature T_c^0.

According to CNT, $s_c \propto |h_p|^{-d}$ and therefore at any fixed T, stronger fields will allow many critical droplets to form and hence the system goes over to the MD regime. On the other hand, a weaker field rules out the possibility of more than one critical droplet and therefore the system goes over to the SD regime.

Figure 9 shows snapshots of the spin configurations at different times in both SD and MD regimes. The snapshots at $t = t_0 + \Delta t$ corresponds to $m_w \sim O\left(10^{-2}\right)$. $h_p > h_{DSP}$ in figure 9(a) and a single large droplet is formed whereas $h_p < h_{DSP}$ in (b) and many droplets are seen to be formed. It may be noticed from figure 9 that the boundaries of the droplets are flat with very few kinks on it at $t = t_0 + \Delta t$. The probability of growth of a droplet along a flat boundary is very small (only 25% in case of a square lattice) and hence domain wall movement practically stops immediately after the withdrawal of the field. This restricts further nucleation. It is then left to very large fluctuations to resume the domain wall movement and long time is required for the system to come out of the metastable state and subsequently reach the final equilibrium state. Thus the effect of the pulse is to initiate the nucleation process and the threshold value of the pulse strength is such that within the pulse duration it renders the system with droplets almost without any kink in it. This observation justifies the sharp growth of the relaxation time at the phase boundary.

The growth of a length scale at the transition phase boundary can be qualitatively shown from the distribution of domains of reversed spins. We define a pseudo-correlation length $\widetilde{\xi}$ as

$$\widetilde{\xi}^2 = \frac{\sum_s R_s^2 s^2 n_s}{\sum_s s^2 n_s}, \tag{26}$$

where the radius of gyration R_s is defined as $R_s^2 = \sum_{i=1}^{s} \left|r_i - r_0\right|^2 / s$, r_i denoting the position vector of the ith spin of the domain and $r_0 = \sum_{i=1}^{s} r_i / s$ being the centre of mass of the domain. As the transition phase boundary is approached, $\widetilde{\xi}$ is observed to grow with the system size as shown in figure 10. Typical number of MCR used for obtaining the data is 10 for $L = 1000$ and 2000 for $L = 50$. This indicates the divergence of a length scale at the phase boundary in the thermodynamic limit. It should be noted, however, that $\widetilde{\xi}$ is not exactly the correlation length of the system [18]. An estimate for the power law growth of the actual correlation length ξ, as the phase boundary is approached in the MD region, will be obtained from the finite size scaling study discussed later in this section.

The order of the magnetization-reversal transition changes with temperature and with Δt even along the same phase boundary. The transition is discontinuous all along the low T phase boundary, whereas at higher values of T the nature of the transition changes from a continuous to a discontinuous one as one moves towards higher values of Δt. For $h_p^c(T) \ll h_{DSP}(T)$, the system is brought to the SD regime where the order of the transition is observed to be discontinuous. On the other hand continuous transition is observed for $h_p^c(T) \gg h_{DSP}(T)$ when the system goes over to the MD regime. One can look at the probability distribution $P(m_w)$ of m_w to determine the order of the phase transition. Figure 11 shows the variation of $P(m_w)$ as the phase boundary corresponding to a particular

temperature is crossed at two different positions (different Δt). The data are averaged over 500 MCR. The existence of a single peak in (a), which shifts its position continuously from $+1$ to -1 as the phase boundary is crossed, indicates the continuous nature of the transition. In (b), however, two peaks of comparable strength at positions close to $\pm m_0$ exist simultaneously. This shows that the system can simultaneously reside in both the phases which is a sure indication for a discontinuous phase transition. On phase boundaries corresponding to higher temperatures the crossover from the discontinuous transition to a continuous one is not very sharp and there exists a region around $h_p^c = h_{DSP}$ on the phase boundary, over which the nature of the transition cannot be determined with certainty. This is evident from figure 7, where the data points near the tricritical point do not fit to the slope of either of the straight lines corresponding to the two different regimes.

In the region where the transition is continuous in nature one can expect scaling arguments to hold. We assume power law behaviour in this regime both for m_w

$$m_w \sim \left| h_p - h_p^c \left(\Delta t, T \right) \right|^{\beta} \tag{27}$$

and for the correlation length

$$\xi \sim \left| h_p - h_p^c \left(\Delta t, T \right) \right|^{-\nu} . \tag{28}$$

For a finite size system, h_p^c is a function of the system size L. Assuming that at the phase boundary ξ can at the most reach a value equal to L, one can write the finite size scaling form of m_w as [19] :

$$m_w \sim L^{-\beta/\nu} f \left[\left(h_p - h_p^c \left(\Delta t, T, L \right) \right) L^{1/\nu} \right], \tag{29}$$

where $f(x) \sim x^{\beta/\nu}$ as $x \to \infty$. A plot of $m_w / L^{-\beta/\nu}$ against $\left(h_p - h_p^c \left(\Delta t, T, L \right) \right) L^{1/\nu}$ shows a nice collapse of the data corresponding to $L = 50$, 100, 200, 400 and 800 for $d = 2$ and $L = 10$, 20, 40, 80 and 120 for $d = 3$ as shown in figure 12. Typical number of MCR used to obtain the data is 5120 for $L = 50$ in $d = 2$ and 10000 for $L = 10$ in $d = 3$. The values of the critical exponents obtained from the data collapse are $\beta = 0.85 \pm 0.05$ and $\nu = 1.5 \pm 0.5$ in $d = 3$ and $\beta = 1.00 \pm 0.05$ and $\nu = 2.0 \pm 0.5$ in $d = 2$, where $h_p^c \left(\Delta t, T \right)$ was obtained with an accuracy $O \left(10^{-3} \right)$. All attempts to fit similar data to the above finite size scaling form obtained in the SD regime failed.

The accuracy with which $h_p^c \left(\Delta t, T \right)$ is measured, is very crucial for obtaining the critical exponents through finite size scaling. The cumulant method introduced by Binder et al. [20] is one of the reliable methods which can be employed to obtain the value of h_p^c. The fourth order cumulant is defined as

$$g(L) = \frac{1}{2} \left[3 - \frac{\langle m_w^4 \rangle}{\langle m_w^2 \rangle^2} \right], \tag{30}$$

where $\langle m_w^n \rangle = \int m_w^n P(m_w) dm_w$. The quantity $g(L)$ is dimensionless and is equal to unity for $|m_w| \gg 0$, while $g(L) \to 0$ for $m_w \to 0$, assuming a Gaussian distribution of m_w around 0 on the phase boundary. Figure 13 shows a plot of $g(L)$ against h_p at a fixed Δt and T and the value of the pulse strength corresponding to the point of intersection of the different curves gives $h_p^c(\Delta t, T)$; assuming $g \equiv g\left[L/\left|h_p - h_p^c\right|^{-\nu}\right]$. Typical number of MCR used to obtain the data is 50000 for $L = 50$ and 2500 for $L = 800$. It is to be noted that none of the curves touch the abscissa which corresponds to $m_w = 0$ which is numerically unattainable. The closer one gets to $m_w = 0$ better the accuracy in the measurement of h_p^c. In principle the minima of $g(L)$ correponding to different L should occur at the same position (at $h_p = h_p^c$). The shift in the position of the minima of $g(L)$ in figure 13 is caused by the presence of large fluctuations in measuring higher moments of m_w. However, this estimate of h_p^c, when used in the scaling fit of (29), did not significantly improve the estimates of the critical exponents β and ν.

4 Summary and Conclusions

In this paper we have discussed in detail almost all the studies that have been made so far on the dynamic magnetization-reversal transition in the Ising model under finite duration external magnetic field competing with the existing order for $T < T_c^0$. Any combination of the pulse strength and duration above the phase boundary in the $h_p - \Delta t$ plane leads to the transition from one ordered phase to the equivalent other. We solved numerically the mean field equation of motion for the magnetization to obtain the MF phase boundary where the susceptibility and the relaxation time were observed to diverge. The divergence of both the time (τ_R^{MF}) and the length scale (ξ^{MF}) at the MF phase boundary was observed even from the analytic solution of the MF equations of motion under a linear approximation. Under this approximation, the dynamical critical exponent was found to have a value 2 : $\tau_R^{MF} \sim \left(\xi^{MF}\right)^2 \sim -\ln|m_w|$, where $m_w\left(h_p, \Delta t, T\right) = 0$ gives the phase boundary. The same transition has been studied using Monte Carlo simulations in both two and three dimensions. The obtained phase diagram is fully consistent with the classical nucleation theory. The nucleation process is initiated by the external magnetic field and depending on the strength of the field the system nucleates either through the growth of a single droplet or through the growth and subsequent coalescence of many droplets. For $h_p > h_{DSP}$ the system belongs to the multi-droplet regime and the transition is continuous in nature; whereas for $h_p < h_{DSP}$ the system goes over to the single-droplet regime where transition is discontinuous. Expecting power law behaviour for both m_w and ξ in multi-droplet regime, the finite size scaling fits give the estimates of the critical exponents β and ν for both $d = 2$ and 3. Unlike in the MF case, where the relaxation time τ_R^{MF} shows a logarithmic divergence, τ_R in MC studies falls off

exponentially away from $m_w = 0$ and the divergence in τ_R comes through the growth of the prefactor κ in (25) with the system size.

The symmetry breaking transition of the dynamic hysteresis in pure Ising systems under oscillating external fields [1][5][6], where the $m - h$ loop becomes asymmetric due to the fact that the magnetization $m(t)$ fails to follow even the phase or sign of the rapidly changing field $h(t)$, leads to a dynamic transition. This dynamic transition has been studied employing finite size scaling theory [6][7] and the estimates of the critical exponents seem to be consistent with the static Ising universality class [21]. Although this transition as well as the one discussed in this paper occur due to the failure of the system to get out of the 'free energy well' corresponding to the existing order because of the lack of proper combination of the pulse strength and duration, they belong to different universality classes.

Acknowledgements

We are grateful to M. Acharyya, D. Chowdhury, C. Dasgupta, B. Duenweg, D. Stauffer and R. B. Stinchcombe for their useful comments and suggestions.

References

[1] Chakrabarti B K and Acharyya M 1999 *Rev. Mod. Phys.* **71** 847

[2] Sides S W, Rikvold P A and Novotny M A 1998 *Phys. Rev.* E **57** 6512

[3] Misra A and Chakrabarti B K 1998 *Phys. Rev.* E **58** 4277

[4] Tome T and de Oliveira M J 1990 *Phys. Rev.* A **41** 4251

[5] Acharyya M and Chakrabarti B K 1995 *Phys. Rev.* B **52** 6550

[6] Sides S W, Rikvold P A and Novotny M A 1998 *Phys. Rev. Lett.* **81** 834

[7] Sides S W, Rikvold P A and Novotny M A 1999 *Phys. Rev.* E **59** 2710

[8] Acharyya M, Bhattacharjee J K and Chakrabarti B K 1997 *Phys. Rev.* E **55** 2392

[9] Misra A and Chakrabarti B K 1997 *Physica* A **247** 510

[10] Stinchcombe R B, Misra A and Chakrabarti B K 1999 *Phys. Rev.* E **59** R4717

[11] See e.g., Gunton J D and Droz M 1983 *Introduction to the Theory of Metastable and Unstable States* (Heidelberg : Springer)

[12] Suzuki M and Kubo R 1968 *J. of Phys. Soc. Japan* **24** 51

[13] See e.g., Binder K 1984 *Application to the Monte-Carlo Method in Statistical Physics* (Heidelberg : Springer)

[14] Blöte H W J, Luijten E and Heringa J R 1995 *J. Phys.* A **28** 6289

[15] Rikvold P A, Tomita H, Miyashita S and Sides S W 1994 *Phys. Rev.* E **49** 5080

[16] Acharyya M and Stauffer D 1998 *Euro. Phys. J.* B **5** 571

[17] Misra A and Chakrabarti B K 2000 arXiv:cond-mat/0002085

[18] Stinchcombe R B 1985 *Scaling Phenomena in Disordered Systems* ed. Pynn R and Skeljorp A (New York : Plenum)

[19] See e.g., Barber M N 1983 *Phase Transition and Critical Phenomena* eds. Domb C and Lebowitz J L (New York : Academic)

[20] See e.g., Binder K and Heermann D 1988 *Monte Carlo Simulation in Statistical Physics* (Berlin : Springer-Verlag)

[21] Rikvold P A, Korniss G, White C J, Novotny M A and Sides S W 2000 *Computer Simulation Studies in Condensed Matter Physics* XII eds. Landau D P et. al. (Berlin : Springer)

Figure Captions

Figure 1. Typical time variation of the response magnetizations $m(t)$ for two different field pulses $h(t)$ with same Δt and T are shown. The quantities of interest to characterize the response magnetizations for both the pulses are indicated.

Figure 2. MF phase boundaries for three different temperatures. The solid line is obtained from numerical solution of (7) and the dotted lines give the corresponding analytical estimates in the linear limit.

Figure 3. Logarithmic divergence of τ_R^{MF} across the phase boundary for $T/T_c = 0.9$. The data points shown by circles are obtained from the solution of (7) and the solid line corresponds to the solution of the linearized MF equation.

Figure 4. Divergence of $\chi_{q=0}$ across the phase boundary obtained from the numerical solution of (17).

Figure 5. Plot of χ_q against m_w for different values of q. The inset shows the linear variation of $\left(\xi^{MF}\right)^{-2}$ against $[\ln|m_w|]^{-1}$. The data points for ξ^{MF} in the inset are obtained from the slope of the best fitted straight lines through a plot of $\ln\chi_q$ against q^2 for different values of m_w.

Figure 6. Phase boundaries obtained from the MC study for (a) square lattice with $L = 100$ and (b) simple cubic lattice with $L = 50$.

Figure 7. Plot of $\ln\Delta t$ against $(h_p)^{1-d}$ along the MC phase boundary. (a) $T/T_c = 0.31$ and (b) $T/T_c = 0.09$ for square lattice and (c) $T/T_c = 0.67$ and (d) $T/T_c = 0.11$ for simple cubic lattice. The slope ratio $R \simeq 3.27$ in (a) and $\simeq 3.97$ in (c).

Figure 8. MC results for the divergence of τ_R for $L = 40$, 50, 100, 200 and 400. The best fitted straight lines are guide to the eye. The inset shows the variation with L of the peak height κ in the prefactor of τ_R in (25).

Figure 9. Snapshots of spin configurations in a 100×100 square lattice at different stages ($t = t_0$, t_1 and $t_0 + \Delta t$) of nucleation, where $t_0 < t_1 < t_0 + \Delta t$. The dots correspond to $+1$ spin state. (a) $h_p = 0.55$, $\Delta t = 300$ at $T/T_c = 0.44$ (SD regime) and (b) $h_p = 0.52$, $\Delta t = 9$ at $T/T_c = 0.88$ (MD regime).

Figure 10. Variation of $\widetilde{\xi}$ with L for $L = 50$, 100, 200, 400, 800 and 1000 for MC study on a square lattice.

Figure 11. Plot of $P(m_w)$ against m_w as one crosses the phase boundary for the MC study on a 100×100 square lattice in (a) MD regime and (b) SD regime.

Figure 12. Finite size scaling fits : (a) for $d = 2$ at $T/T_c = 0.88$ and (b) for $d = 3$ at $T/T_c = 0.67$.

Figure 13. Plot of $g(L)$ against L for $L = 50$, 100, 200, 400 and 800 in the MD regime for MC study on a 100×100 square lattice at $T = 2.0$ for $\Delta t = 5$.

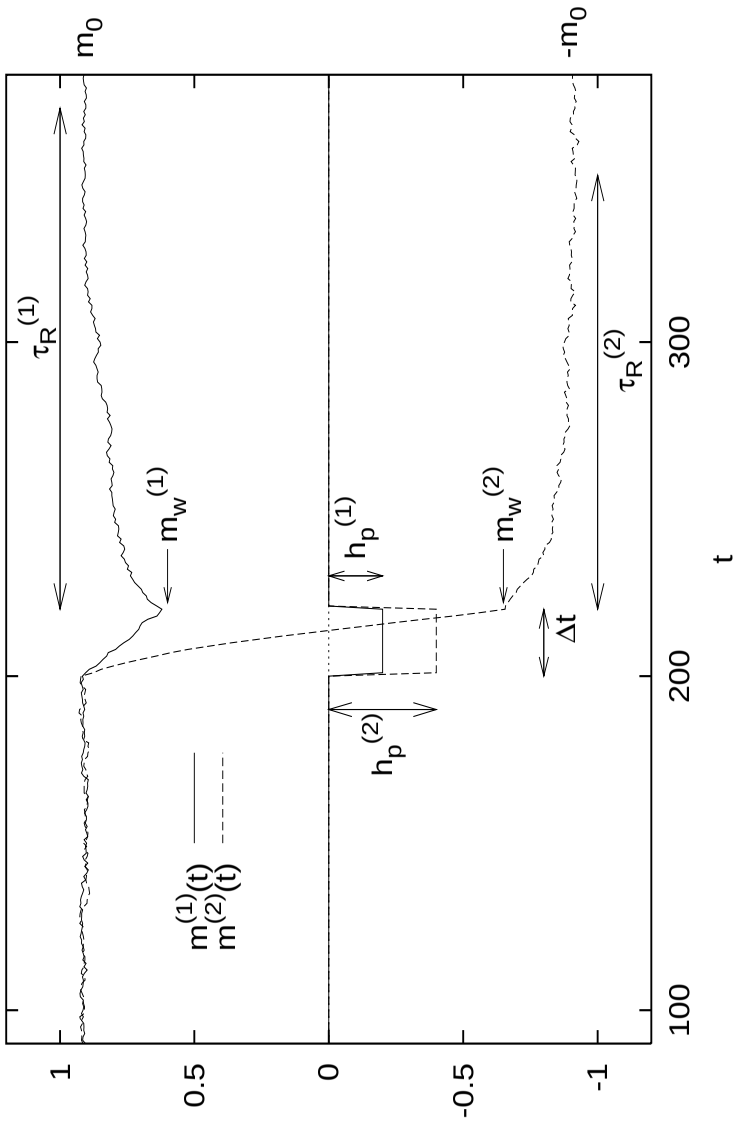

Figure 1.

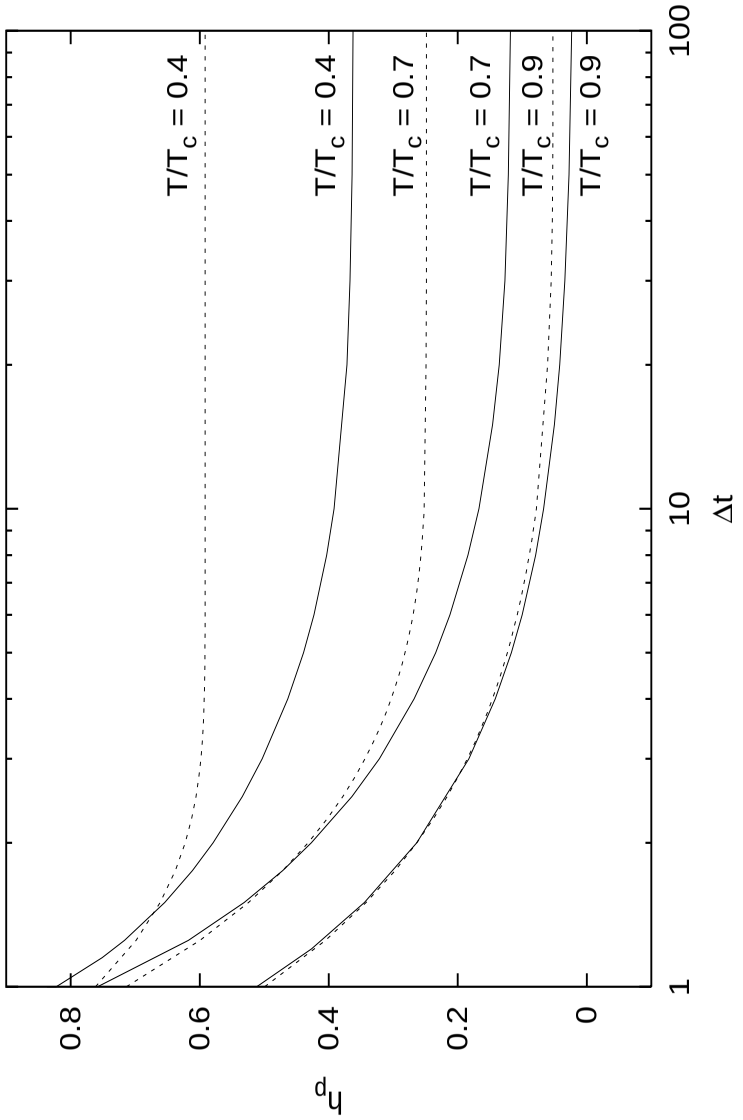

Figure 2.

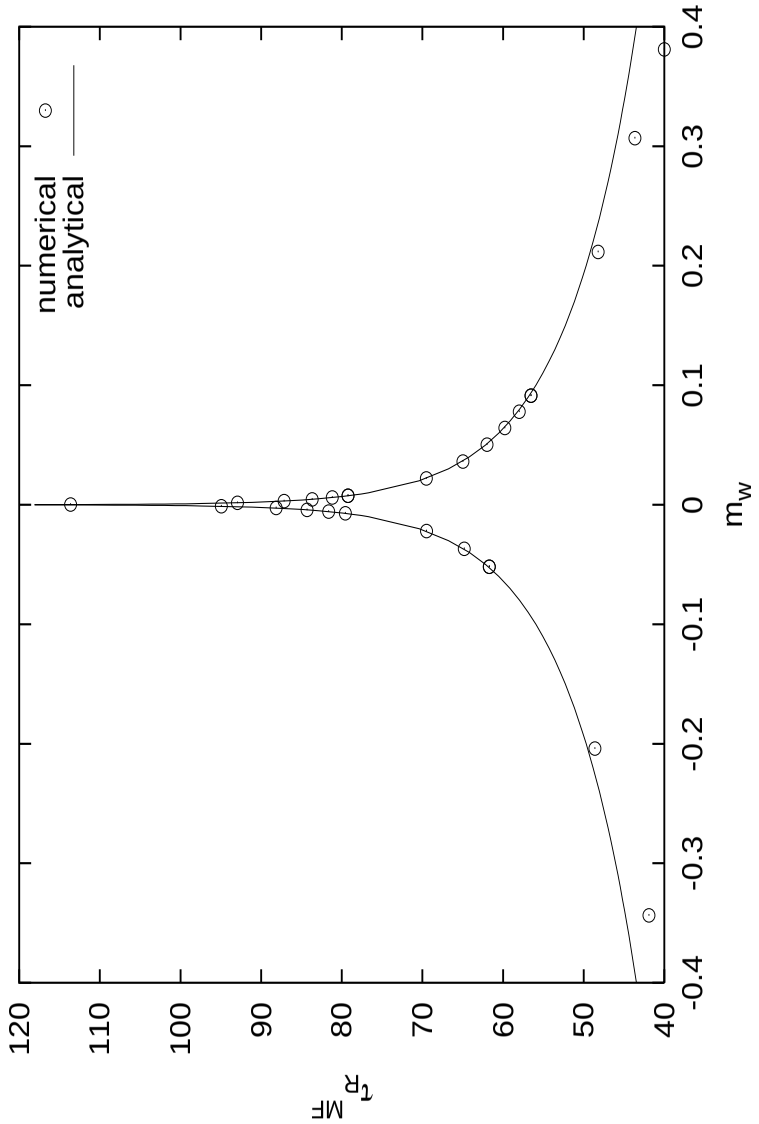
numerical
analytical
τ_{RMF}
m_w
120
110
100
90
80
70
60
50
40
-0.4
-0.3
-0.2
-0.1
0
0.1
0.2
0.3
0.4

Figure 3.

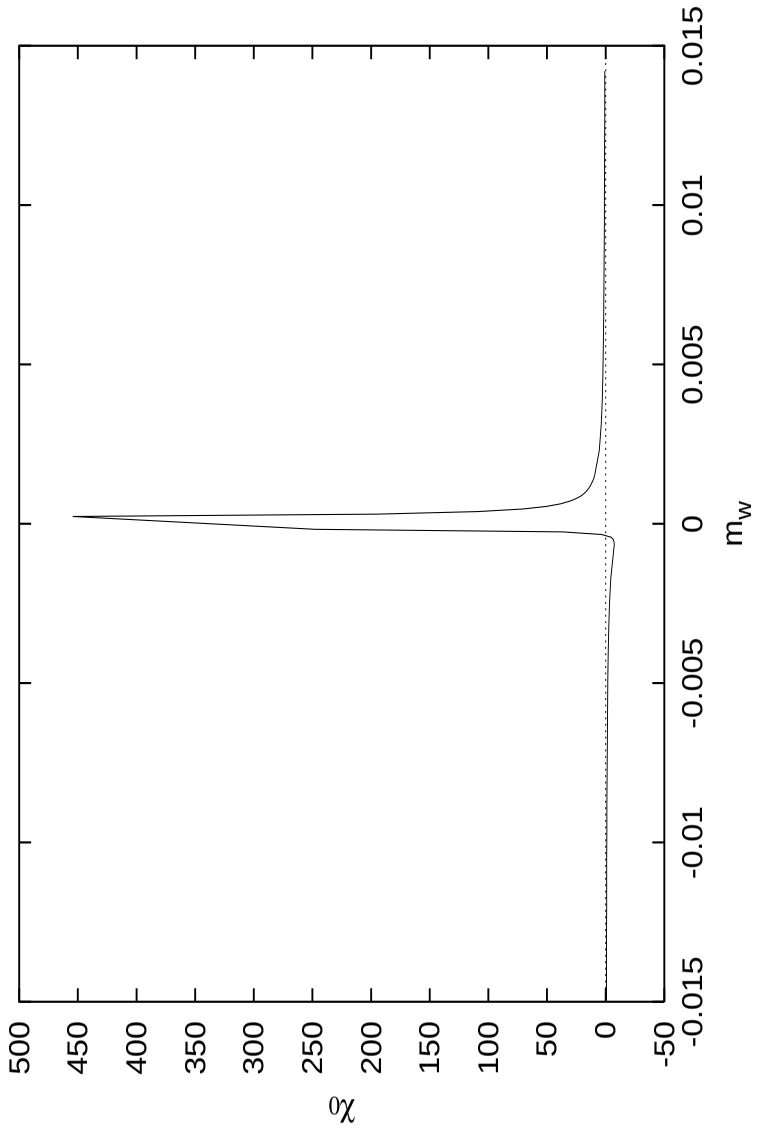
500
450
400
350
300
250
200
150
100
50
0
-50
χ_0
0.015
0.01
0.005
0
-0.005
-0.01
-0.015
m_w

Figure 4.

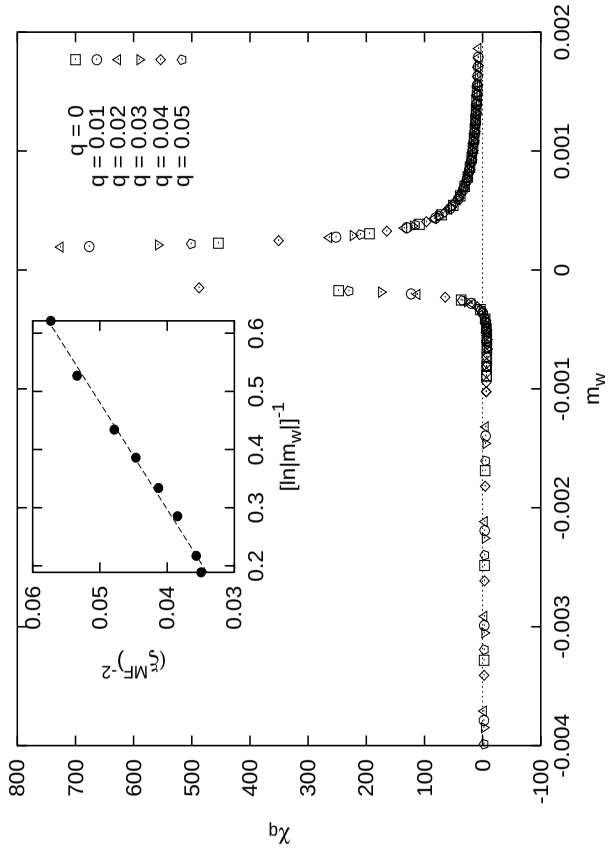

Figure 5.

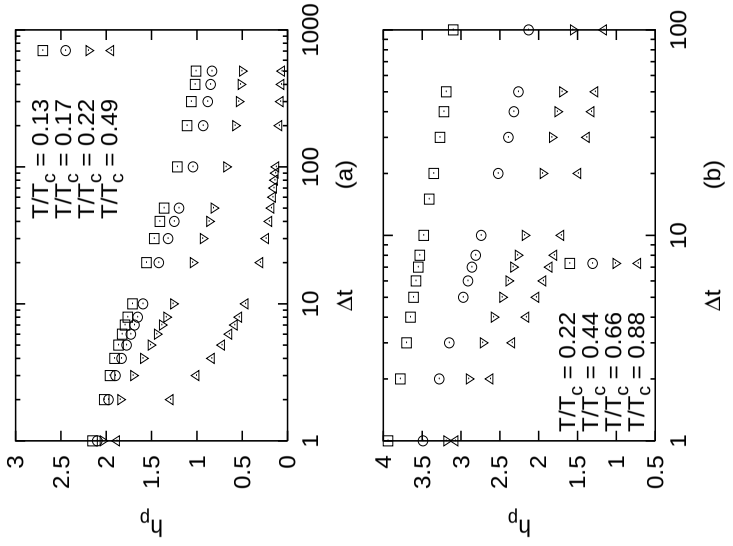
T/T_c = 0.13
T/T_c = 0.17
T/T_c = 0.22
T/T_c = 0.49
h_p
Δt
(a)
T/T_c = 0.22
T/T_c = 0.44
T/T_c = 0.66
T/T_c = 0.88
h_p
Δt
(b)

Figure 6.

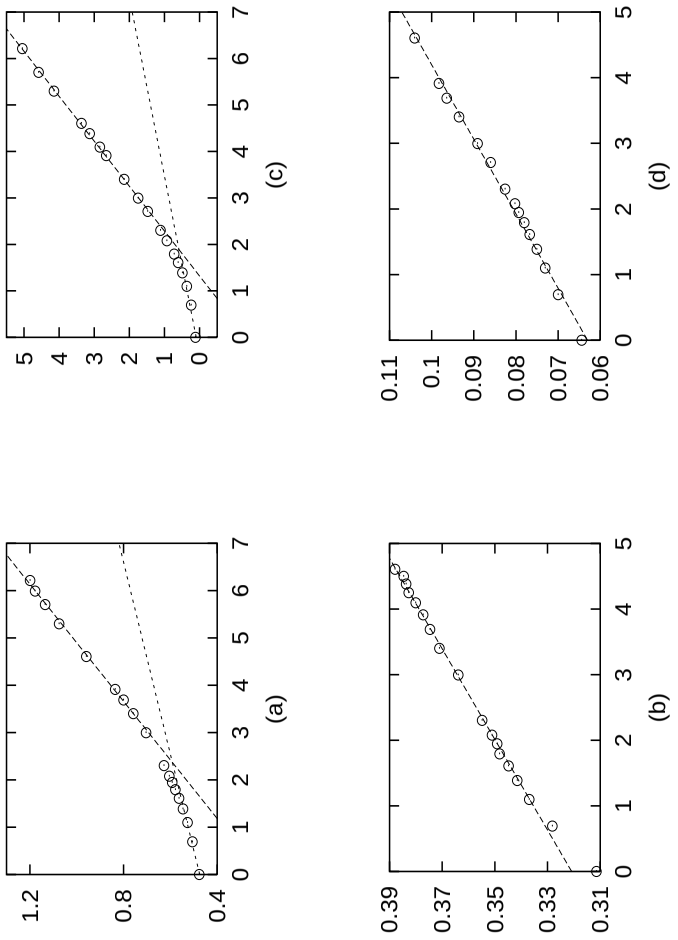

Figure 7.

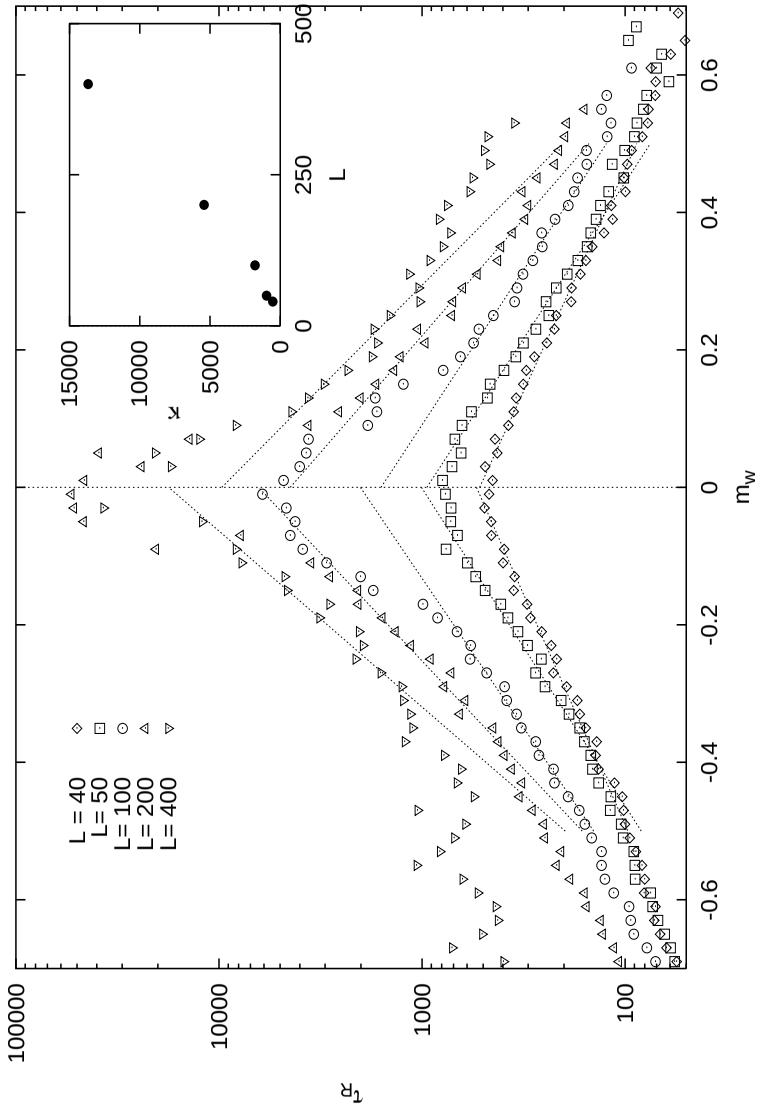
100000
10000
1000
100
τ_R
-0.6
-0.4
-0.2
0
0.2
0.4
0.6
m_w
L = 40
L= 50
L= 100
L= 200
L= 400
15000
10000
5000
0
κ
0
250
500
L

Figure 8.

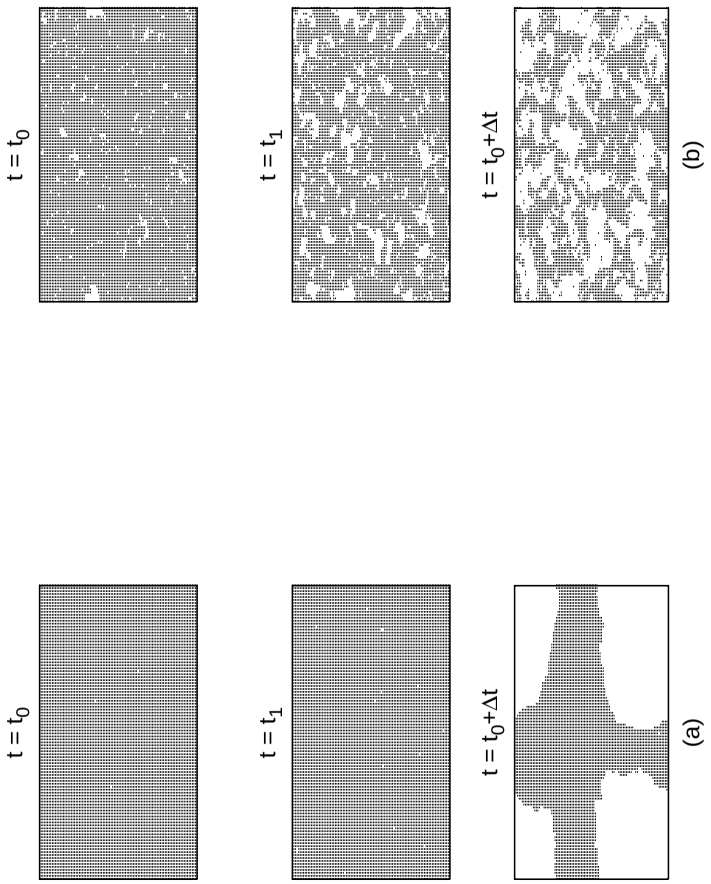

Figure 9.

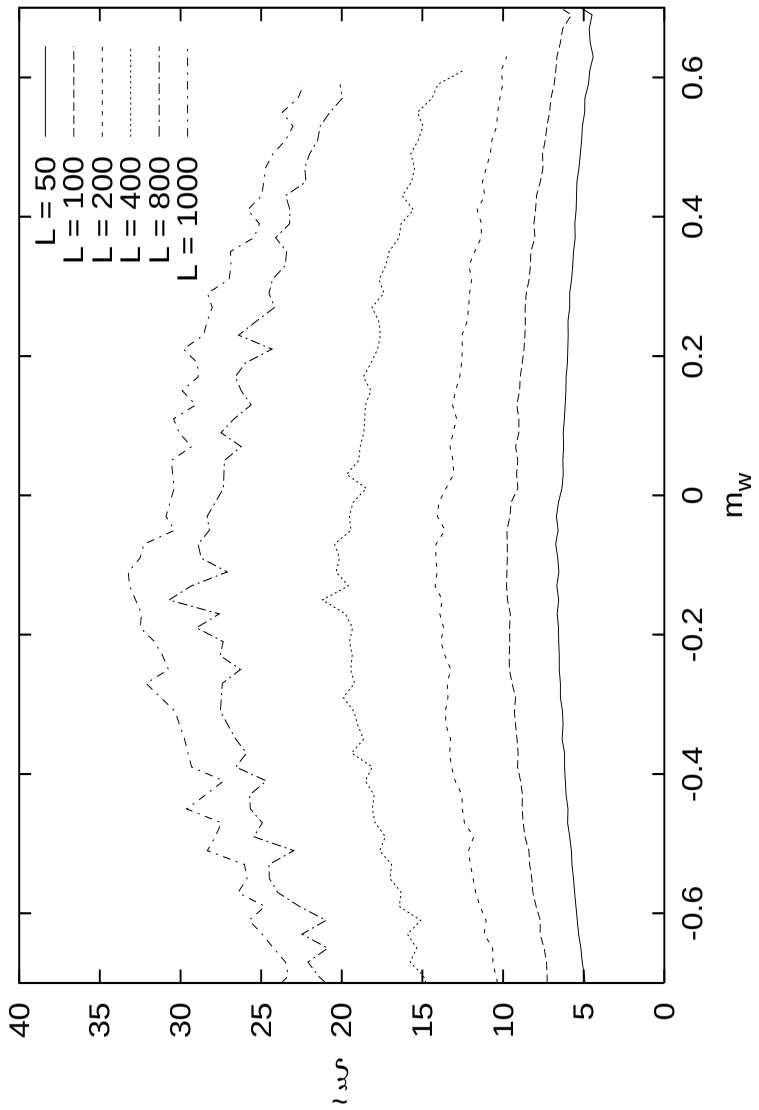
L = 50
L = 100
L = 200
L = 400
L = 800
L = 1000
40
35
30
25
20
15
10
5
0
-0.6
-0.4
-0.2
0
0.2
0.4
0.6
m_w

Figure 10.

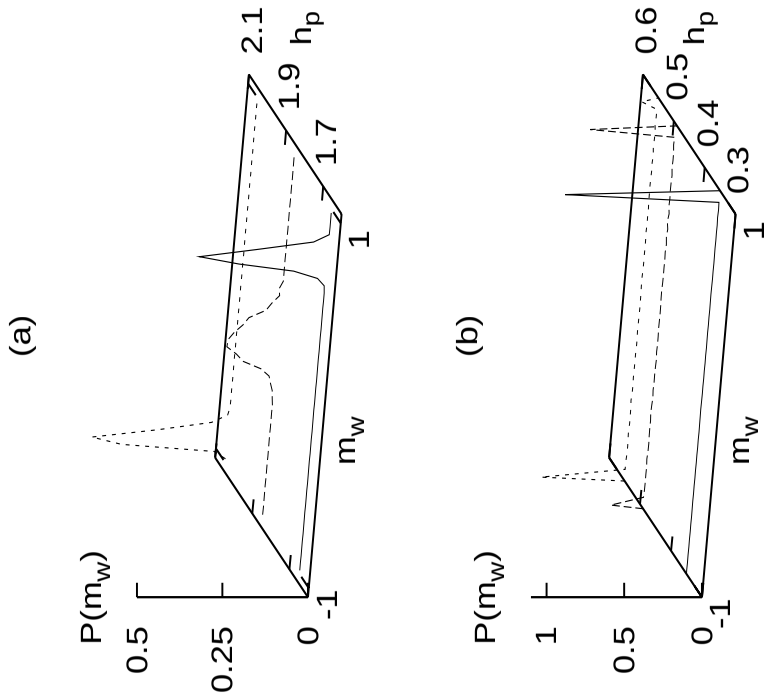

Figure 11.

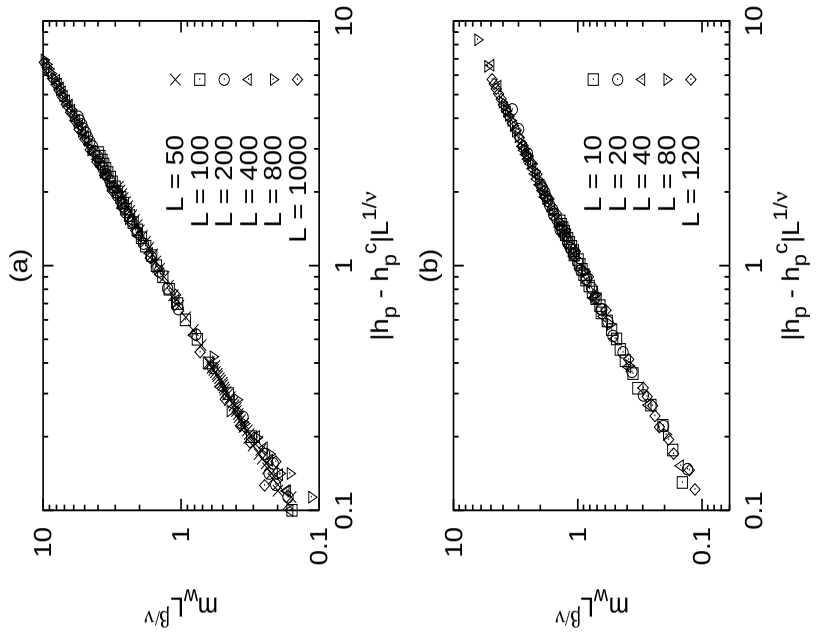
(a)
(b)
L = 50
L = 100
L = 200
L = 400
L = 800
L = 1000
L = 10
L = 20
L = 40
L = 80
L = 120
10
1
0.1
0.1
1
10
$m_W L^{\beta/\nu}$
$|h_p - h_p^c| L^{1/\nu}$

Figure 12.

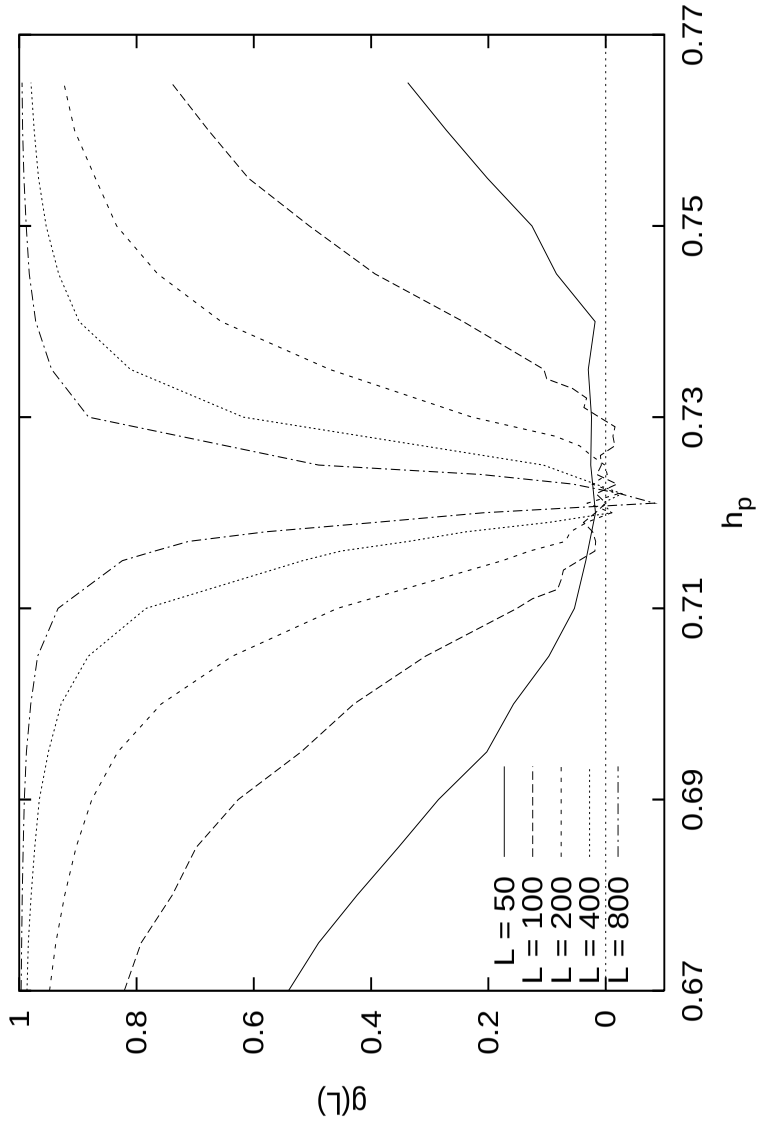
g(L)
1
0.8
0.6
0.4
0.2
0
0.67
0.69
0.71
0.73
0.75
0.77
h_p
L = 50
L = 100
L = 200
L = 400
L = 800

Figure 13.